Range Prediction for a Three Wheel Plug-in Hybrid Electric Vehicle

Nicolas Denis, Maxime R. Dubois, Karol Angarita Gil, Thomas Driant, Alain Desrochers
Sherbrooke University, Engineering Faculty, Sherbrooke, Canada
deninic@cta-brp-udes.com

***Abstract*- Plug-in hybrid electric vehicles (PHEV) may carry a high amount of embedded electrical energy and provide the possibility to recharge it while not running. As a consequence, they will exhibit a relatively long distance in full electric mode. Many kind of electric or hybrid vehicles are available or about to be developed. This paper presents a new concept of a three wheel recreational PHEV and its achievable performance. It will first describe the topology and model of the vehicle, and then we will provide results on its all electric range (AER) over a normalized drive cycle.**

I. INTRODUCTION

The vehicle geometry described in this paper has intrinsic properties that influence all the process of hybridization. In a three-wheel vehicle, the frontal area is larger than for a conventional (two-wheel) motorcycle, which means that the aerodynamic performance will be affected. Secondly, this vehicle offers more space than conventional motorcycles to store electrical energy but less than a standard four wheel vehicle. Since literature on plug-in hybrid three-wheel vehicles barely exists, we propose an electrical range prediction for this type of vehicle. A previous work gave some interesting hints for the range prediction of a plug-in hybrid small scooter [1], also we propose a complete model for a three-wheel vehicle with a different electrical architecture. The paper will first describe the topology of the three-wheel vehicle investigated. Sections III and IV of the paper will describe the mathematical model used for the vehicle force modeling. Section V will investigate accessories consumption and its influence on battery discharge. Finally we will present some results on the vehicle full electric range on a normalized speed cycle.

II. TOPOLOGY

The three-wheel vehicle investigated in the paper has a parallel hybrid topology, providing long distance range in hybrid mode and short distance range in a pure electric mode. The full hybrid drive train is illustrated in Fig. 1 and is slightly different from the small scooter drive train described in [1]. The continuously variable transmission (CVT) of the smaal scooter is replaced by a conventionnal fixed ratios gearbox. This can be justified by the fact that a classical low cost CVT is unefficient and cannot be driven. Moreover high performance CVTs exist but are very expensive compared to a classical gearbox.

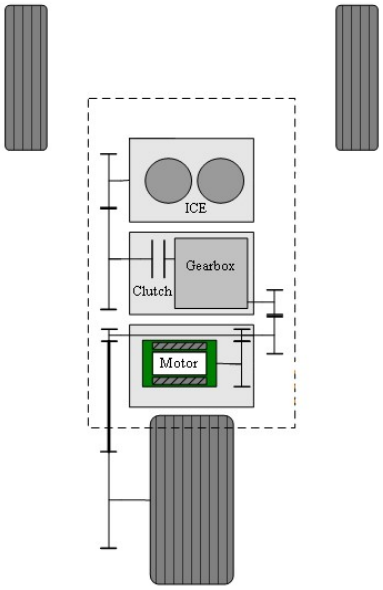

Fig. 1. Full power train configuration.

This paper will focus on the available range in the full electric mode. Thus, we will describe the electric power train configuration only, the latter illustrated in Fig. 2. A battery pack delivers the bus voltage to an voltage-source inverter which converts DC voltage into a sinusoidal three phases AC voltage for the electric motor. The motor is connected to the main shaft by a first gear, then the main shaft provides mechanical power to the rear wheel through the final belt in

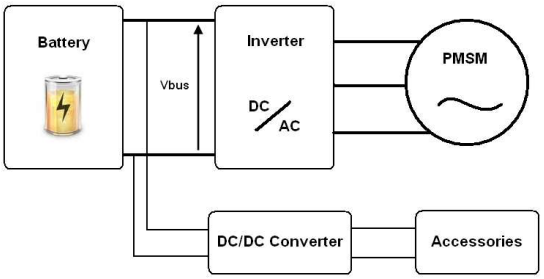

Fig. 2. Electric power train configuration.

order to reduce the operating speed to the rear wheel.

The two-wheel scooter discussed in [1] has less available space for the battery compared to the three-wheel motorcycle discussed here. With a 100 liters battery volume available this will enable an enhanced range in full electric mode, as the battery pack will store as much as 4.5 kWh of electrical energy. The total embedded electrical energy of the scooter [1] was 0.5 kWh and its range was 15 km in pure electric. In both cases, Lithium-Ion cells are considered.

Contrary to [1], the choice is made to eliminate the DC/DC converter between the battery and the inverter. This choice will allow more volume to be allocated to the battery. Therefore the bus voltage is not regulated and depends on battery state of charge (SOC), the efficiency of both motor and inverter will depend on the variation of the bus voltage, which are all modeled in the paper.

The electromechanical technology is also different between the two motorcycles. The scooter uses a salient poles permanent magnet synchronous motor (PMSM) while the three-wheel motorcycle uses non-salient poles PMSM. Non-salient poles PMSM are easy to control. Salient poles PMSM will have the advantage of reduced copper losses in flux-weakening operation but are more difficult to control. The motor described in this paper is chosen with the requirements of allowing pure electric mode on a highway cycle.

Finally, the large three-wheel motorcycle allows a bigger battery pack and a electrical motor and gasoline engine with higher power, but it badly impacts the weight of the vehicle. The three-wheel motorcycle is more than four time heavier than the scooter of [1]. Moreover the two front wheels of the three-wheel motorcycle sharply increase the frontal area.

III. MECHANICAL MODEL

In view of the final results desired in this study, which is to establish a procedure for the range prediction of a three-wheel vehicle, a complete loss model needs to be put forward. First the mechanical loss model is presented.

The mechanical model provides the required rear wheel torque based on the information on vehicle speed. This model uses the global equation

$$T_w = r\left[f_{mec}(v) + \left(\frac{J_{tot}}{m_v r^2} + 1\right) m_v \frac{dv}{dt}\right], \qquad (1)$$

where T_w is the rear wheel torque, v is the vehicle speed, r is rear wheel radius, J_{tot} is the total inertia of the wheels and m_v is the vehicle mass.

The function f_{mec} represents the resistance force on the vehicle and is the sum of aerodynamic drag (f_{drag}) and rolling resistance (f_{roll}).

$$f_{drag}(v) = \frac{1}{2}\rho_a C_d A_f v^2, \qquad (2)$$

$$f_{roll}(v) = m_v g(f_{r0} + f_{r1} v + f_{r2} v^2), \qquad (3)$$

where ρ_a is the air density, C_d is the aerodynamic drag coefficient, A_f is the frontal area of the vehicle, f_{r0}, $f_{r1}$and f_{r2} are respectively the zero, first and second order coefficients of the rolling resistance.

IV. ELECTRICAL MODEL

The compilation of all losses also require that electrical losses in the PM synchronous machine and inverter be considered.

A. Motor

A permanent magnet synchronous motor was chosen because it offers a good tradeoff between power and volume. Space sharing between the engine, the motor/inverter and the battery is a main concern on two-wheel and three-wheel motorcycles, also the chosen dimensions for the electrical machine are an axial length of 243 mm for an outer diameter of 152 mm. The other specifications are a maximum continuous power of 12 kW, a peak power of 21 kW and a base speed of 3000 rpm. It is assumed that the motor will have non-salient poles, sinusoidal back EMF, star connected stator windings and vector control. In a permanent magnet synchronous motor, the main losses are core and copper losses [2].

1. Hysteresis losses

Core losses (hysteresis and eddy current losses) are caused by the magnetic flux variations in iron. Since the rotor moves together with the rotating field, we make the assumption that iron losses are negligible in the rotor back iron. A complete estimation of the machine losses would need to consider the harmonics caused by the teeth in the magnets, especially at higher speeds. However, this investigation is left for further studies. As a consequence, in this paper, all the core losses are localized in the stator teeth and yoke.

The magnetic behaviour of iron can be described by an hysteresis cycle. If we define *B* as the magnetic flux density and *H* as the magnetic field intensity in the stator laminations, the couple (*B*,*H*) of the iron goes all over the hysteresis cycle during an electrical period. This phenomenon causes hysteresis losses that increase with the frequency. Generally, hysteresis losses can be written

$$p_h = K_h \left(\frac{f}{50Hz}\right)\left(\frac{\hat{B}}{1.5T}\right)^n, \qquad (4)$$

where p_h is the laminations specific hysteresis losses in W/kg, f is the electrical frequency, $\hat{B}$ is the peak value of the magnetic flux density in the stator yoke and n is the Steinmetz constant (n = 2 is considered in our case). Here K_h is chosen as 5 W/kg at 50 Hz and 1.5 T.

The flux linkage flowing in the stator coil on a per phase basis is λ_l, which is the sum of the magnet flux and the windings flux linking the windings. If the winding resistance is neglected, the phase voltage can be written

$$u(t) = \frac{d\lambda_l}{dt}. \qquad (5)$$

The frequency spectrum of the phase voltage is composed of a low frequency component at frequency f and a high frequency component due to the switching frequency of the inverter. If the high frequency content is neglected and a sinusoidal phase voltage is assumed, the flux linkage can be written

$$\lambda_l(t) = -\frac{U\sqrt{2}}{2\pi f} cos(2\pi f t), \tag{6}$$

where U is the rms value of the stator phase voltage. Two cases need to be considered.

At low speed, the inverter allows a flexible variation of the phase voltage. In that region, the motor does not need flux weakening and the U/f ratio is kept constant. According to eq. (6), this strategy will make the amplitude of the flux linkage λ_l constant, leading to a constant value of $\hat{B}$. According to eq. (4), this will give: hysteresis losses are proportional to f and then to motor speed N,

$$P_h \propto N\,. \tag{7}$$

With a base speed of 3000 rpm, a 4 pole motor of stator mass 25 kg will give P_h = 360 W.

At high speed, above the base speed, the inverter output voltage is limited by its DC bus voltage and U is kept constant. To keep control of the motor torque, flux weakening technique is required. According to eq. (6), a constant voltage U and an increasing frequency will give decreasing values of λ_l and decreasing values of $\hat{B}$. Thus, above the base speed, hysteresis losses can be written

$$P_h \propto \frac{1}{N}\,. \tag{8}$$

The hysteresis losses have their highest values at the base speed.

2. Eddy current losses

In addition to the hysteresis losses, the variation of the magnetic flux inside the stator will induce eddy current in the stator yoke laminations. Generally, the eddy current specific losses (in W/kg) can be written

$$p_{ed} = K_{ed}\left(\frac{f}{50Hz}\right)^2\left(\frac{\hat{B}}{1.5T}\right)^n\,, \tag{9}$$

where K_{ed} is a material dependent coefficient. Here K_{ed} is chosen as 1.3 W/kg at 50 Hz and 1.5 T.

With the same reasoning as discussed in section 1, the eddy current losses are, at low speed,

$$P_{ed} \propto N^2\,, \tag{10}$$

giving, at 3000 rpm a loss value of 187 W.

Above the base speed, in the flux weakening area, equation (9) will give

$$P_{ed} \propto U^2\,. \tag{11}$$

As U is kept constant, the eddy current losses are constant in that speed range.

3. Copper losses

In the three-phase frame, the stator currents and voltages can respectively be written

$$\begin{pmatrix} i_a \\ i_b \\ i_c \end{pmatrix} = I\sqrt{2}\begin{pmatrix} -\sin(\theta+\varphi_i) \\ -\sin\left(\theta-\frac{2\pi}{3}+\varphi_i\right) \\ -\sin\left(\theta+\frac{2\pi}{3}+\varphi_i\right) \end{pmatrix}, \tag{12}$$

$$\begin{pmatrix} u_a \\ u_b \\ u_c \end{pmatrix} = U\sqrt{2}\begin{pmatrix} -\sin(\theta+\varphi_u) \\ -\sin\left(\theta-\frac{2\pi}{3}+\varphi_u\right) \\ -\sin\left(\theta+\frac{2\pi}{3}+\varphi_u\right) \end{pmatrix}, \tag{13}$$

where I and U are respectively the rms values of stator current and phase voltage, θ is the electrical angle and φ_i and φ_u are respectively the stator current and voltage phases.

The transformation to the rotor frame (d,q) is made by using the Concordia transformation first and then the Park transformation. The Concordia transformation uses the matrix T_{32}^t and the Park transformation uses the matrix $P_{-\theta}$ defined by

$$T_{32}^t = \sqrt{\frac{2}{3}}\begin{pmatrix} 1 & -\frac{1}{2} & -\frac{1}{2} \\ 0 & \frac{\sqrt{3}}{2} & -\frac{\sqrt{3}}{2} \end{pmatrix}, \tag{14}$$

$$P_{-\theta} = \begin{pmatrix} cos\,\theta & sin\,\theta \\ -sin\,\theta & cos\,\theta \end{pmatrix}. \tag{15}$$

The corresponding stator current and voltage in the rotor frame are

$$\begin{pmatrix} I_d \\ I_q \end{pmatrix} = P_{-\theta} * T_{32}^t * \begin{pmatrix} i_a \\ i_b \\ i_c \end{pmatrix} = I\sqrt{3}\begin{pmatrix} -sin\,\varphi_i \\ cos\,\varphi_i \end{pmatrix}, \tag{16}$$

$$\begin{pmatrix} U_d \\ U_q \end{pmatrix} = P_{-\theta} * T_{32}^t * \begin{pmatrix} u_a \\ u_b \\ u_c \end{pmatrix} = U\sqrt{3}\begin{pmatrix} -sin\,\varphi_u \\ cos\,\varphi_u \end{pmatrix}. \tag{17}$$

In the (d,q) frame, the electrical equations in steady state are

$$\begin{cases} U_d = RI_d - X_s I_q \\ U_q = RI_q + X_s I_d + E_q \end{cases}, \tag{18}$$

where R is the stator resistance, X_s is the stator reactance and E_q is the no-load line voltage. The rotor is assumed to be non-salient, that is X_s is kept constant.

The expression of electrical active power per phase is given by

$$U_d I_d + U_q I_q = R\left(I_d^2 + I_q^2\right) + E_q I_q\,, \tag{19}$$

and is the sum of the copper losses $R\left(I_d^2 + I_q^2\right)$ and the electromagnetic power $E_q I_q$. Moreover core losses contribute to brake the shaft and we can relate current and torque by the equation

$$E_q I_q = TN + P_{ed} + P_h \,, \qquad (20)$$

where T is the mechanical torque.

At low speed I_d is usually set to zero because this part of the current creates copper losses, but does not provide any mechanical power. E_q is proportional to the motor rotational speed N and the quadrature current I_q can easily be determined using (20). At high speed, above the base speed, the limitation of the bus voltage requires that I_d be different from zero, to account for flux-weakening. I_d can be determined from (18), with the constraint that

$$U_d^2 + U_q^2 = constant \,. \qquad (21)$$

As a consequence of increasing I_d, copper losses will increase at high speed. Fig. 3 presents the Fresnel diagrams for these two differents cases.

Finally it is possible to use (18), (20) and the constraint on bus voltage in order to relate output variables (speed and torque) and input variables (stator currents and voltages).

Fig 4., Fig 5. and Fig 6. respectively show the q-axis stator current, the d-axis stator current and the copper losses evolution with the motor speed for different torque profiles. The first torque profile is the maximum torque available depending on motor speed. The second torque profile is half the first one and the last one is the zero torque profile. We used a constant bus voltage of 350 V, a maximum power of 21 kW and a base speed of 3000 rpm which leads to a maximum torque of 67 Nm.

Since the q-axis stator current is nearly proportional to the torque, I_q is constant below the base speed and then decreases with the torque in the constant power range. The d-axis stator current is null at low speed and becomes negative when the stator voltage reaches the bus voltage limitation. The flux weakening operation requires a negative d-axis stator current according to the convention taken in Fig 3.

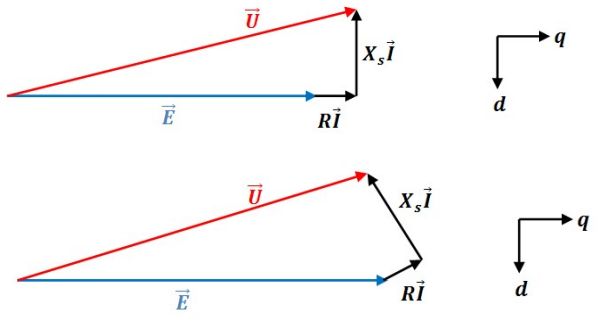

Fig. 3. Fresnel diagram in low speed operation (top) and in flux weakening operation (bottom).

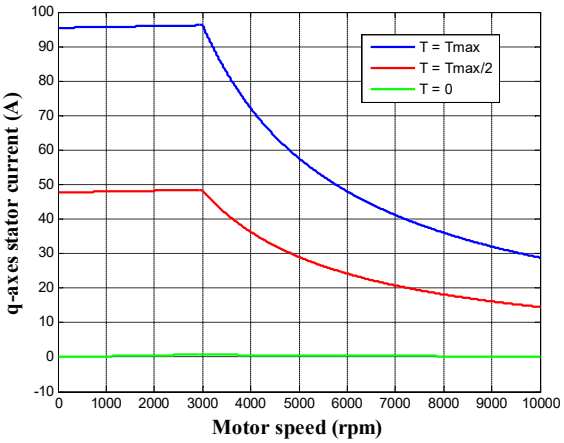

Fig. 4. q-axis stator current evolution with the motor speed.

In flux weakening operation, the copper losses increase since I_d is added to I_q. The worst case appears for the maximum speed and maximum torque and the copper losses are nearly 2200 W. Yet, we observe copper losses of 1720 W in the motor at the highest speed (10,000 rpm) with no torque applied ($T = 0$), due to a high d-axis current.

B. Inverter

The inverter is able to drive the motor by adjusting the stator voltage and frequency. In this study, a conventional three-leg three-level Voltage Source Inverter is used, with Sinusoidal Pulse-Width Modulation. We note M the amplitude modulation ratio. When M varies between 0 and 1, the maximum stator voltage varies between 0 and half of the bus voltage V_{bus}. We assume that stator currents are nearly sinusoidals and we note $\hat{\imath}$ the peak current. The motor inductance and resistance define the phase φ between stator currents and voltages.

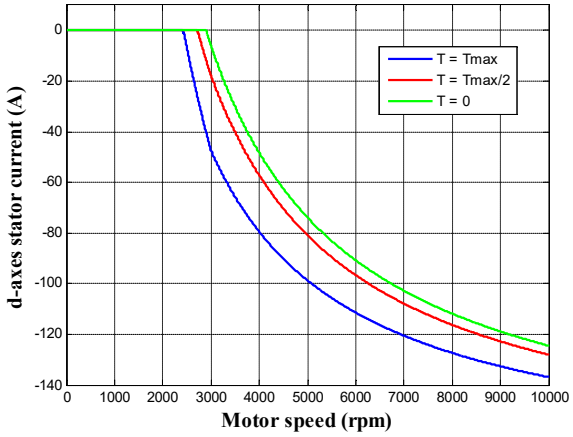

Fig. 5. d-axis stator current evolution with the motor speed.

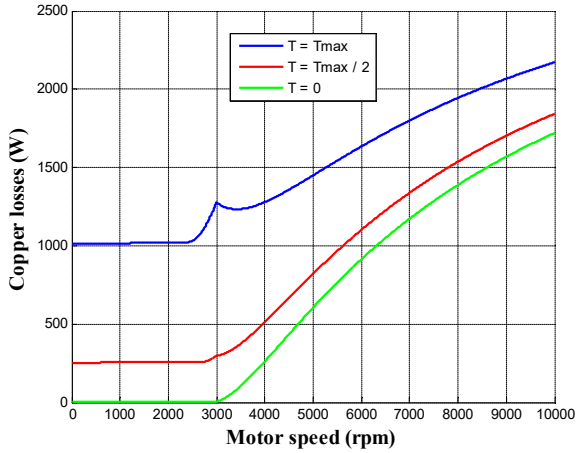

Fig. 6. Copper losses evolution with the motor speed.

1. Conduction losses

Since power switches are not ideal, some power is lost in the inverter. A switch in the ON state sees a voltage drop and the corresponding dissipated power depends on the current going through the device. For a given current, the voltage drop of diodes and IGBTs depends on the threshold voltage V_0 and rated parameters V_N and I_N

$$V_{drop}(i) = \frac{V_N - V_0}{I_N} i + V_0 \,. \tag{22}$$

According to [3], the conduction losses can be written

$$P_c = \left(\frac{1}{8} + \frac{M}{3\pi}\right)\frac{V_N - V_0}{I_N}\hat{\imath}^2 + \left(\frac{1}{2\pi} + \frac{M}{8}cos\varphi\right)V_0\hat{\imath}\,. \tag{23}$$

2. Switching losses

Controlled switches are forced-switched, leading to switching losses proportional to the switching frequency f_s.

The ON switch is characterized by the rated rise time of the current t_{rN} and we can approximate the ON switching losses by

$$P_{on} = \frac{1}{8} V_{bus} t_{rN} \frac{\hat{\imath}^2}{I_N} f_s \,. \tag{24}$$

The OFF switch is characterized by the rated fall time of the current t_{fN}, the corresponding losses are

$$P_{off} = V_{bus}\,\hat{\imath}\,t_{fN}\,f_s\left(\frac{1}{3\pi} + \frac{1}{24}\frac{\hat{\imath}}{I_N}\right). \tag{25}$$

During the OFF switch a diode needs to recover his charge which leads to a short negative peak current in the diode and the corresponding positive peak current in the IGBT. This recovery current, together with the voltage through the device, leads to additional losses.

Diodes and IGBTs that are considered in the model are characterized by the parameters shown in Table I. Fig 7.

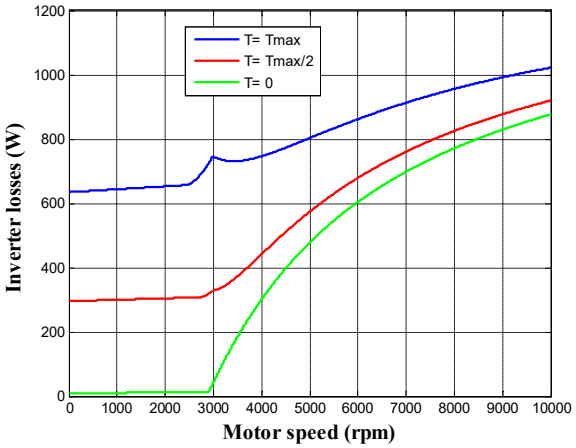

Fig. 7. Inverter losses evolution with the motor speed.

shows the evolution of inverter losses with the motor speed for the three different torque profiles seen before. Again, a voltage bus of 350 V was used. Finally, this model allows us to determine the input power of the inverter thanks to the input variables of the motor.

C. Battery

Naturally, the vehicle estimated range will increase with the capacity of the battery but a strong constraint in our case is the limited space. The battery pack is designed to deliver the required bus voltage while limiting the drawn current of the cells.

The cell is modeled by a voltage source E in series with a resistance R_{int}, E depends on the cell SOC [4] and can be written

$$E = E_0 - K\frac{Q}{Q - it}Ae^{-B\,it}\,, \tag{26}$$

where A, B, K, E_0 are constant that have to be estimated experimentaly, Q is the total capacity of the cell and it is the consumed capacity of the cell.

TABLE I
INVERTER PARAMETERS

IGBT	
Rated collector current	400 A
Rated collector-to-emitter voltage	3 V
Threshold collector-to-emitter voltage	1 V
Rated rise time	700 ns
Rated fall time	1000 ns
Diode	
Rated diode forward voltage	2 V
Diode threshold voltage	0.8 V
Rated recovery charge	10^{-6} C
Rated recovery time	200 ns
Switching frequency	15 kHz

To be closer to the reality, we used correction factors to take temperature and current into account [5]. We use the correction factors k_1 and k_2 to have a more accurate estimation of the consumed capacity it

$$it = \int_0^t k_1[i(u)].k_2[T(u)].i(u)\,du\,. \qquad (27)$$

Moreover the open circuit voltage of the cell is corrected using the correction factor k_3

$$V_{cell} = E(it) - R_{int}i(t) + k_3[T(t)]\,. \qquad (28)$$

The three factors have been evaluated experimentaly. The resistance is evaluated using a three dimensional table that depends on temperature, current and SOC. Equations (26), (27) and (28) allows us to determine the bus voltage, then we can approximate the drawn current of the battery pack thanks to the the input power of the inverter.

V. ACCESSORIES CONSUMPTION

The vehicle accessories need a non negligible amount of power at all time that will not be used to propel the vehicle. Table II shows the consumption of the main accessories and separates the case low speed and high speed.

On a one hour ride in the city, accessories will consume 0.430 kWh. If the nominal capacity of the battery is 4.5 kWh, this means that accessories will consume 9.6% of the battery capacity over this trip.

VI. RESULTS

Using the analytic model presented above, a simulation tool has been developed using MATLAB/SIMULINK computing environment. A simulation were performed in full electric mode on successive FTP urban cycles, the battery state of charge is assumed to be 95% charged at the beginning of the cycle and the simulation is stopped when state of charge reaches 30%. The evolution of the SOC over the driving cycle is given on the Fig. 8.

Our results show that the vehicle completes 45.9 km before SOC drops to the 30% level. Fig. 9 shows the estimation of the different power losses in the vehicle.

VII. CONCLUSION

Based on the existing literature, the paper proposes an original complete model of a new concept of three wheel vehicle in order to estimate AER and losses in the whole power train.

TABLE II
ACCESSORIES CONSUMPTION

	Low speed	High speed
Lights	138 W	123 W
Power steering	84 W	36 W
Cooling	136 W	118 W
Controllers	47 W	47 W
	…	…
Total	430 W	380 W

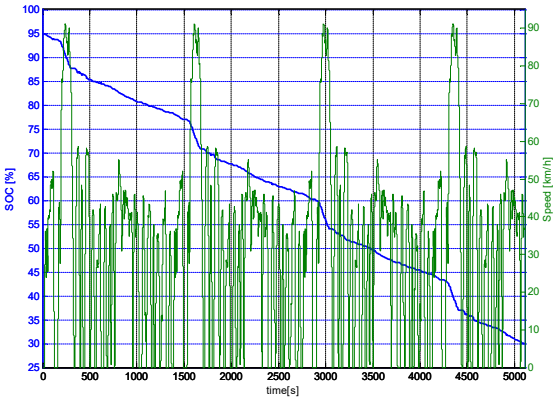

Fig. 8. SOC evolution over the speed cycle. SOC (%) in blue and speed (km/h) in green.

The previous study shows that the plug-in hybrid small scooter allows a pure electric range of 20 km. The design of the three-wheel vehicle offers more space for the battery and the electric motor, as a consequence the investigated three-wheel vehicle can increase this range up to 46 km despite an increase of volume and mass.

The results show that approximately 54% of the total delivered energy is used to directly propel the vehicle and the other 46% are lost in brakes, drive train, motor, inverter, battery and accessories. All of these results will be key data for future developments of the vehicle.

REFERENCES

[1] M. Ceraolo, A. Caleo, P. Capozzella, M. Marcacci, L. Carmignani, and A. Pallottini, "A Parallel-Hybrid Drive-Train for Propulsion of a Small Scooter," *IEEE Trans. On Power Electronics,* vol. 21, no. 3, pp. 768-778, May 2006.

[2] R. Krishnan, *Permanent Magnet Synchronous and Brushless DC Motor Drives,* Boca Raton, Florida, 2010.

[3] F. Casanellas, "Losses in PWM inverters using IGBTs," *IEE Proc.-Electr. Power Appl.*, vol. 141, no. 5, pp. 235-239, September 1994.

[4] O. Tremblay, L-A. Dessaint, A-I. Dekkiche, "A Generic Battery Model for the Dynamic Simulation of Hybrid Electric Vehicles," *IEEE Vehicle Power and Prop. Conf.,* pp. 284-289, 2007.

[5] L. Gao, S. Liu, and R.A. Dougal, "Dynamic Lithium-Ion Battery Model for System Simulation," *IEEE Trans. On Components And Packaging Tech.,* vol. 25, no. 3, pp. 495-505, September 2002.

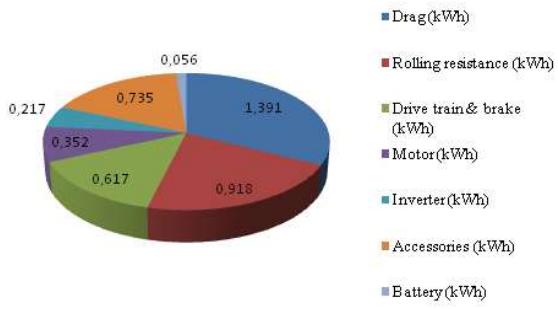

Fig. 9. Pie chart for losses estimation.